Fluctuation-Driven Transport in the DIII–D Boundary

D.L. Rudakov,[1] J.A. Boedo,[1] R.A. Moyer,[1] S. Krasheninnikov,[1] A.W. Leonard,[2] M.A. Mahdavi,[2] G.R. McKee[3], G.D. Porter,[4] P.C. Stangeby,[5] J.G. Watkins,[6] W.P. West,[2] D.G. Whyte[1] and G. Antar[1]

[1]*University of California, San Diego, La Jolla, California 92093-0417*

[2]*General Atomics, San Diego California 92186-5608*

[3]*University of Wisconsin, Madison, WI, 53706*

[4]*Lawrence Livermore National Laborabory, Livermore California*

[5]*University of Toronto Institute for Aerospace Studies, 4925 Dufferin St., Toronto, M3H 5T6, Canada*

[6]*Sandia National Laboratories, Alberqueue, New Mexico*

Abstract. Cross-field fluctuation-driven transport is studied in edge and scrape-off layer (SOL) plasmas in the DIII–D tokamak using a fast reciprocating Langmuir probe array allowing local measurements of the fluctuation-driven particle and heat fluxes. Two different non-diffusive mechanisms that can contribute strongly to the cross-field transport in the SOL of high-density discharges are identified and compared. The first of those involves intermittent transport events that are observed at the plasma separatrix and in the SOL. Intermittence has qualitatively similar character in L-mode and ELM-free H-mode. Low-amplitude ELMs observed in high-density H-mode produce in the SOL periods with cross-field transport enhanced to L-mode levels and featuring intermittent events similar to those in L-mode. The intermittent transport events are compatible with the concept of plasma filaments propagating across the SOL due to $E \times B$ drifts. Another type of non-diffusive transport is often seen in high-density H–modes with prolonged ELM-free periods, where the transport near the separatrix is dominated by quasi-coherent modes driving particle and/or heat fluxes exceeding L-mode levels. Those modes may play an important role by providing particle and/or heat exhaust between ELMs.

1. Introduction

It is widely believed that electrostatic turbulence is responsible for most of the cross-field particle and heat transport in the tokamak edge plasma (see e.g. [1] and references therein). This has been confirmed by direct measurements of turbulent $E \times B$ transport in a number of experiments (see e.g. [1-5]). However, the physical mechanisms behind the turbulent cross-field transport are not yet fully understood.

A fast reciprocating Langmuir probe array [6] has been previously used in DIII-D [7] to study turbulent particle transport in Ohmic, L and H-modes of operation. The results were compared to particle fluxes obtained from the 2-D local transport code UEDGE [8]. In many cases the measured fluxes exceeded those from UEDGE by a large enough factor to allow for a substantial asymmetry in the turbulent fluxes [4]. In particular, in L-mode and H-mode with no edge localized modes (ELMs, see [9] for review) the turbulent flux measured at the outboard mid-plane exceeded flux-surface-averaged flux from UEDGE by factors of 18 and 4.5, respectively [4]. Moreover, far scrape-off-layer (SOL) density profiles were often found to be nearly flat [10, 11], particularly in high-density L-modes [12]. This implies either very high cross-field diffusion coefficients increasing towards the wall or non-diffusive character of the cross-field transport.

Recent results from DIII-D [12] and other devices [13] indicate that intermittent events play significant role in the cross-field particle transport. In this paper we will present some further analysis of intermittent transport in DIII-D, including heat transport as well. Though intermittence is observed under broad variety of plasma conditions [12], in absolute terms it has largest effect at higher densities. Therefore here we will limit ourselves to considering high-density L and H-modes. In addition to L-mode and ELM-free H-mode conditions discussed in previous work [12] we will consider fluctuation-induced transport during ELMs

as well as certain conditions when the transport is dominated by quasi-coherent modes rather than intermittence.

2. Description of experiments

A description of the mid-plane reciprocating probe on DIII-D can be found elsewhere [6]. The probe is inserted into the plasma horizontally, its axis laying 18.8 cm below the mid-plane of the machine (see Fig. 1(a)). The total in-and-out (plunge) time is about 0.2 s. The total plunge length (from the outermost to the innermost point) is about 15 cm. A typical position trace for the inner part of the plunge is shown in Fig. 1(b). Here R_{sep} is the major radius of the separatrix (calculated by the toroidal equilibrium fitting code EFIT [14]) at the probe location (see Fig. 1(a)). Radial profiles of the plasma parameters measured by the probe are produced by plotting a corresponding time series smoothed over a short time interval (so that the probe motion can be neglected, typically 1 ms) against the distance from the separatrix measured along the probe insertion chord: $\Delta R_{sep} = R_{probe} - R_{sep}$.

A fast (100 kHz bandwidth) electron temperature diagnostic [15, 16] has been recently installed on the probe array. The technique is based on detection of harmonics generated in the current spectrum of a single Langmuir probe driven by high-frequency sinusoidal voltage. The diagnostic on DIII-D features fully digital data analysis and active voltage feedback [16].

The tip layout on the probe head (Fig. 1(c)) has been modified for the experiments described below to allow simultaneous measurements of the turbulent (electrostatic) particle, convective heat and conductive heat fluxes given respectively by [5, 17]:

$$\Gamma_r^{ES} = \frac{1}{B_j}\langle nE_q \rangle \tag{1}$$

$$Q_r^{ES} = Q_{conv} + Q_{cond} = \frac{3}{2} kT_e \Gamma_r^{ES} + \frac{3}{2}\frac{n_e}{B_j}\langle kT_e E_q \rangle . \tag{2}$$

Of the five available probe tips three poloidally separated tips are used to measure the floating potential (V_f) and the remaining two are used for the ion saturation current (I_{si}) and electron temperature (T_e) measurements. The arrangement of the tips allows an estimate of the poloidal electric field in two different locations:

$$E_{q1} \approx (V_{f1} - V_{f2})/a \ , \ \ E_{q2} \approx (V_{f3} - V_{f1})/a \, , \tag{3}$$

where a is the tip separation. E_{q1} is then used to correlate with I_{si} to obtain the the turbulent particle flux and convective heat flux, while E_{q2} is used to correlate with T_e (obtained by harmonic technique) for the conductive heat flux measurements. Plasma density n_e is derived from I_{si} and T_e in the usual way[1]:

$$n_e \approx -2 I_{si} \left(\sqrt{2kT_e / M_i} A_p e \right)^{-1} , \tag{4}$$

where A_p is the probe collecting area, M_i is the ion mass and e is the electron charge. Here we are assuming that ion and electron temperatures are equal: $T_i = T_e$.

3. Experimental results

a. Fluctuation levels and turbulent fluxes in L and H-mode

A series of experiments aimed at the best possible documentation of the edge parameters of L-mode plasmas in DIII-D has been recently conducted. A few H-mode discharges were produced at comparable conditions. The data presented below was obtained in Lower Single Null (LSN) magnetic configuration with plasma current $I_p \approx 1 - 1.5$ MA, toroidal magnetic field at the magnetic axis $B_0 \approx 1.5 - 2$ T, comparatively low neutral beam injection (NBI) heating power $P_{NBI} \approx 0.5 - 2$ MW, and high line-average plasma density $\bar{n}_e = 0.6 - 1.1 \times 10^{14}$ cm^{-3}. The Greenwald density factor for the discharges shown below was about

0.85 – 1. A typical poloidal cross-section of the magnetic configuration (calculated by EFIT) is shown in Fig. 1(a).

Figure 2 shows radial profiles (versus the distance from the separatrix) of time-averaged (over 1 ms) electron density (a), electron temperature (b), and their respective absolute root-mean-square (RMS, denoted by "~") (c,d) and relative (e,f) fluctuation levels in L and H-mode discharges. The shaded region represents an uncertainty of the probe position with respect to the separatrix, mostly due to EFIT limitations. One should note that such profiles contain both spatial and temporal information, thus apparent modulation on some of the signals in far SOL is probably due to non-stationary processes rather than radial variation. Temporal information can be eliminated by averaging the profiles over a few probe plunges under similar conditions. However, obtaining completely reproducible probe plunges is not always possible, particularly in H-mode discharges with ELMs. On the other hand, keeping some temporal information may be beneficial to illustrate different conditions (for example between and during ELMs) in the same plot. Here we will use single plunge profiles while keeping in mind the limitations.

Fig. 2 contains data from three different discharges: an L-mode discharge (open circles) and two H-mode discharges, both featuring ELMs. The first H-mode discharge (solid diamonds) with NBI power P_{NBI} = 1.7 MW had relatively long ELM-free periods. A single ELM occurred when the probe was about 7 cm outside the LCFS, and then there were no ELMs until the probe reached the separatrix (for about 30 ms). The other H-mode discharge (open squares + line), similar to the first one but with lower NBI power P_{NBI} = 0.75 MW, had lower amplitude (by about a factor of 7 - 10 from D_a) but more frequent ELMs. About five of those can be seen in Fig. 2.

The L-mode density and temperature profiles are quite typical for high density conditions: a comparatively fast decay by a factor of 2 for n_e and a factor of about 4 for T_e within the first centimeter from the separatrix and then nearly flat, decreasing by only a factor

of 2 over the next 7 centimeters. In both H-mode cases temperatures and densities near the separatrix are close to L-mode values. The initial decay for both temperature and density between ELMs is faster than in L-mode. In the far SOL (ΔR_{sep} > 3 cm) the density between ELMs is 5 – 10 times lower than in L-mode, while the temperature is lower by 30-50%. During ELMs both density and temperature increase to near L-mode values or even above (temperature), depending on the ELM amplitude.

Fluctuation levels of both n_e and T_e are lower between ELMs in H-mode than they are in L-mode. However, during ELMs in the near SOL (ΔR_{sep} < 2 cm) they increase to or even above L-mode levels. Relative fluctuation levels range from 0.25 – 0.5 for n_e and 0.2 – 0.45 for T_e in most cases except during ELMs when they may reach up to 0.6 – 0.7 for both density and temperature. Between ELMs $\tilde{n}_e / n_e$ is about the L-mode level, while $\tilde{T}_e / T_e$ is slightly lower.

Figure 3 shows radial profiles of the turbulent particle (a,b) and heat (conductive + convective) (c,d) fluxes for the three discharges in linear (a,c) and semi-log (d,e) scale. Both fluxes are higher in L-mode through most of the SOL than they are in H-mode between ELMs. In the rapidly ELMing H-mode (open squares + line) both fluxes increase during ELMs, reaching L-mode levels in the near SOL (ΔR_{sep} < 3 cm). Modulation by ELMs is also clearly visible further out. Remarkably, in the slow ELMing H-mode (solid diamonds) during a larger amplitude ELM the fluxes reach L-mode level even in the far SOL ($\Delta R_{sep} \approx$ 7 cm). In both H-mode cases particle flux near the separatrix is slightly above and the heat flux is about twice higher than those in L-mode.

b. Intermittence in fluctuations and fluxes

The fluxes in Fig. 3 were calculated in time domain according to eqs. (1, 2) by taking an ensemble average of products of the corresponding quantities. They include contributions

from fluctuations with frequencies between 1 kHz and 500 kHz. In this section we will characterize time-resolved fluxes and try to trace their origin.

Figure 4 shows time traces of the electron density, electron temperature and poloidal electric field as well as time-resolved turbulent particle and heat fluxes. The fluxes are obtained according to eqs. (1-2), but without averaging. All records are 1 ms long; each point in Figs. 2 and 3 is averaged over a similar interval. Shown are the data from 2 discharges used in Figs. 2 and 3: the L-mode discharge and the slowly ELMing H-mode discharge (solid diamonds in Figs. 2, 3). The distance from the separatrix is similar in both cases.

Intermittent bursts with amplitudes of 2 – 4 times the average level are evident on all signal traces. Direct comparison reveals that bursts in n_e, E_q and (sometimes) T_e are often correlated. This produces higher relative amplitude spikes in the turbulent fluxes. In absolute terms burst amplitude of n_e and E_q is about twice as large in L-mode as in H-mode while T_e burst amplitudes are comparable in both cases. Burst amplitudes of the fluxes are about 4 times higher in L-mode, which is in agreement with Fig. 3.

Previously intermittence in DIII-D was characterized in L-mode and ELM-free periods of H-mode discharges [12]. During ELMs qualitative behavior of the fluctuations and fluxes is often quite similar. Figure 5 presents (in a form similar to that of Fig. 4) signal and flux traces over 1 ms during ELMs (the time window in both cases is shorter than the ELM duration from D_a). The data in the left-hand side are from the rapidly ELMing H-mode discharge from Figs. 2, 3 (open squares) taken when the probe was about 1 cm from the separatrix (during the ELM marked by the second left arrow in Fig. 2 (a)). The data in the right-hand side are from the slowly ELMing H-mode discharge from Figs. 2, 3 (solid diamonds) taken when the probe was about 6.5 cm from the separatrix. In both cases all traces exhibit intermittent bursts similar to those in L-mode and between ELMs. As in L an ELM-free H-mode, spikes in n_e and E_q seem to be well correlated.

Since the bursts in all cases are intermittent and vary in amplitudes and repetition rates, it is convenient to consider an average event. Conditional averaging [18-22] is a powerful tool allowing not only to characterize an average event, but also to check if the events in different signals are correlated. Below we use n_e signal as the primary series for averaging. All events with the relative amplitude above 2.5×RMS fluctuation level ($dn_e / n_e > 2.5\tilde{n}_e / n_e$) are detected within a given time window, then a 0.1 ms interval of the time series about each event is cut out and put in a buffer for subsequent averaging. At the same time similar intervals are cut out of the secondary signals (T_e, E_q , G and Q) and then averaged. Thus, relative phases between the events in different signals are preserved. Conditional averaging results for the data in Figs. 4 and 5 are shown in Fig. 6. For better statistics 2 ms of data were used in each case. For the same purpose a lower threshold of 2.1×RMS level was used for the last case (ELM in far SOL).

Figure 6 confirms some of our previous observations. First of all, average density bursts look quite similar in all four cases. In all cases spikes in electron density are well correlated with those in the poloidal electric field. This results in correlated bursts in both particle and heat (convective) fluxes. The average transport events also look rather similar under all conditions (side bands in the last case, ELM in far SOL, come from the three consecutive large amplitude events that are clearly seen in Fig. 5). On the other hand, the average behavior of the electron temperature varies between different conditions. While in L-mode and ELM-free H-mode there is some degree of correlation between T_e and n_e spikes, it is much weaker than between n_e and E_q. During ELMs T_e and n_e spikes are not correlated at all. Therefore, most of the heat flux carried by the bursts is due to particle convection in all cases.

c. Coherent modes

Another type of fluctuation activity, a quasi-coherent modulation of the plasma density and temperature, often occurs at the separatrix and in near SOL in ELM-free and slowly ELMing high-density H-modes. Figure 7 shows 1 ms of n_e, T_e, E_q traces and time-resolved fluxes near the separatrix ($\Delta R_{sep} \approx 5$ mm) in the slowly ELMing discharge denoted by the solid diamonds in Figs. 2-6. Periodic modulation with frequency of about 18 kHz is clearly seen in all signals. Fluxes behave in a more erratic way, some oscillation periods cause considerably higher transport than the others do. This is probably mostly due to the amplitude difference between consecutive fluctuation periods that multiplies in the fluxes; slight phase differences can also contribute. We use conditional averaging to characterize an average period of the fluctuation. As before, we use n_e as the primary series for averaging and T_e, E_q, G and Q as secondary series. The result is shown in the right-hand side of Fig. 7. In this case oscillations in n_e, T_e and E_q are all well correlated, though there are slight differences in the waveforms. n_e and E_q are modulated roughly in phase, while T_e leads by about 15 μs. All three signals are sufficiently in phase to cause strong transport of particles and heat (both convective and conductive). In absolute terms average particle flux caused by this oscillation is about 50% higher and heat flux is about 3 times higher than the corresponding L-mode values at the same distance from the separatrix (see Fig. 3).

As noted above, coherent activity is often present in H-mode discharges. In the above example it was shown to cause both particle and heat transport exceeding L-mode levels. However, this is not always the case. Figure 8 presents another example of coherent activity occurring in an H-mode discharge with a comparatively long ELM-free period. The upper part of Fig. 8 shows time traces of n_e, T_e and E_q during 4 ms as the probe moves from about 6 mm to about 1 mm outside the separatrix. Periodic modulation is clearly seen in all signals. In this case the fundamental harmonic frequency is about 12.5 kHz. Shown are also time-averaged

(over 1 ms) fluctuation-driven particle and heat fluxes. Convective and conductive components of the heat flux are shown separately. Comparing the maximum fluxes to those in Fig. 3, we can see that while the maximum heat flux roughly matches that near the separatrix in both H-mode cases, the maximum particle flux in the present case is more than an order of magnitude lower (about 25 times). While the modulation amplitude of n_e and T_e in this case is somewhat lower that in the previously considered one (Fig. 7), this alone could not explain the difference in fluxes.

The relative phasing of the modulation in n_e, T_e and E_q can possibly be responsible and thus merits a study. We split the time interval shown in Fig. 8 (a-d) in four consecutive 1 ms intervals and run conditional averaging over each of them. Here we use E_q as the primary signal and n_e and T_e as the secondary ones. Results are shown in the lower part of Fig. 8. Shown are the averaged fluctuating parts of n_e, T_e and E_q normalized to corresponding RMS fluctuation levels (for example, n_e trace is $\left(n_e - \langle n_e \rangle\right)/\tilde{n}_e$). This representation is convenient to highlight the relative phasing of the signals. Notice that in this case it is T_e and E_q that have similar phase while n_e is about 90° out of phase, unlike the data shown in Fig. 7, where modulation in n_e and E_q was roughly in phase while T_e was slightly out of phase. Therefore, the conductive heat flux is high in this case, while the particle flux and convective heat flux are low. The phase shift between n_e and E_q is slightly reduced during the second time interval, and the particle flux starts to increase, but during the next (3^{rd}) time interval the phase shift increases again and the flux is decreased. During the last (4^{th}) time interval the average phase shift between n_e and E_q becomes more than 90° so the particle and convective heat fluxes reverse and become radially inward. However, since the conductive heat flux stays high, the total fluctuation-induced heat flux remains radially outward.

In the above two examples the characteristics of the mode and amplitudes of the associated fluxes depend strongly on the radial location versus the separatrix. Since the probe

is not stationary, it is impossible to say whether that is mostly due to the radial localization of the mode or due to its temporal evolution. This question needs to be resolved by comparison with other diagnostics that can provide longer time records at a given radial location with good enough spatial resolution. However, the results presented above are still valid for each given spatial location at a given time. Regardless of how stationary the mode is, it can still contribute significantly to the cross-field particle and heat transport.

4. Discussion and summary

Fast convection of particles and heat by intermittent bursts has recently attracted much attention [12, 13]. A model involving turbulent formation and radial propagation of high-density plasma filaments or blobs has been proposed [23]. According to this model the blobs are formed near the separatrix (by some mechanism yet to be explained), become polarized by ∇B drift and then propagate outwards due to $E_q \times B_j$ drift. Experimental evidence obtained so far seems to be consistent with this hypothesis. Indeed, correlating spikes in electron density and poloidal electric field in Figs. 4-6 may be interpreted as plasma filaments having density 2-3 times above the background passing by the probe sensors. If we accept this as a working hypothesis, we can estimate an average radial propagation velocity of the blobs from the average poloidal electric field inside the blob as $v_r = E_q / B_j$. Average radial size of a blob can then be estimated as $d_r = v_r \Delta t$ where Δt is an average duration of the spike in n_e, E_q or the time-resolved particle flux (G). In fact, the latter should be more accurate, since it includes both n_e and E_q information. Table 1 summarizes results on the blob velocities and sizes for the data of Fig. 6. Here for Δt we used the width of the spike in G at about 1/3 of the maximum height from the base line (at the base of a broader pedestal). The L-mode values obtained agree with the previous results from the probe and Beam Emission Spectroscopy (BES) diagnostic

[12]. In H-mode blob velocity and size in near SOL are reduced compared to L-mode (by about factors of 2 and 3 between and during ELMs, respectively). Further reduction of the blob velocity and size in far SOL is in agreement with the previous L-mode data [12].

The quasi-coherent modes considered above certainly deserve further study. As we have shown, those modes are capable of driving particle and/or heat fluxes well above the L-mode levels. The origin of those modes is presently not clear. However, some kind of coherent activity is very often (if not always) present in high-density H-mode discharges with prolonged ELM-free periods. Given the high levels of radial transport that those modes can cause, it is possible that they provide enough particle and/or heat exhaust at the plasma edge to prevent the edge gradients from reaching critical values and driving ELMs.

In summary, we have presented experimental evidence for two different non-diffusive mechanisms that can contribute strongly to the cross-field transport in tokamak SOL. Significance and scaling of this non-diffusive transport on particle control and impurity generation is yet to be fully characterized.

Acknowledgements

This research has been supported by U.S. Department of Energy under Grant DE-FG03-95ER54294 and Contracts DE-AC03-99ER54463, W-7405-ENG-48, and DE-AC04-94AL85000. Authors are indebted to the DIII-D Team for operating the tokamak, heating system and diagnostics. Technical support from L. Chousal and R. Hernandez is gratefully acknowledged.

Tables

Condition	E_q (V/m)	v_r (m/s)	Δt (μs)	d_r (cm)
L-mode, near SOL	4000	2500	10	2.5
H-mode, near SOL	2000	1500	10	1.5
ELM, near SOL	1500	1150	7	0.8
ELM, far SOL	650	500	10	0.5

Table 1: Blob velocities and sizes in different conditions (data from Fig. 6). All values are valid within approximately ± 25%

Figure captions

Fig. 1: Diagnostic layout on DIII-D: poloidal location of the mid-plane reciprocating probe (a); typical position trace for the inner part of the probe plunge (b); probe head layout (c).

Fig. 2: Radial profiles of time-averaged (over 1 ms) electron density (a), electron temperature (b), and their absolute RMS (c,d) and relative (e,f) fluctuation levels in L-mode (open circles) slowly ELMing H-mode (solid diamonds) and rapidly ELMing H-mode (open squares + line). Shaded areas represent estimated error in defining the probe position versus the separatrix.

Fig. 3: Radial profiles of the turbulent particle (a,b) and heat (conductive + convective) (c,d) fluxes for the data of Fig. 2 (in linear (a,c) and semi-log (d,e) scale).

Fig. 4: Time traces of the electron density, electron temperature, poloidal electric field and time-resolved turbulent particle and heat fluxes in L-mode and between ELMs in H-mode.

Fig. 5: Time traces of the electron density, electron temperature, poloidal electric field and time-resolved turbulent particle and heat fluxes during ELMs in near and far SOL.

Fig. 6: Conditional averaging results for the signals in Figs. 4-5 with n_e used as the primary series for averaging and T_e, E_q, G and Q as secondary series.

Fig. 7: Time traces of the electron density, electron temperature, poloidal electric field and time-resolved fluctuation-driven particle and heat fluxes during a quasi-coherent mode observed in H-mode discharge marked by solid diamonds in Figs. 2-3. Results of conditional averaging over the time interval featured in the left-hand side are shown on the right.

Fig. 8: Time traces of the electron density, electron temperature, poloidal electric field and time-resolved fluctuation-driven particle and heat fluxes during a quasi-coherent mode in another H-mode discharge. Conditional averaging results for four consecutive 1 ms intervals (marked on the top) with E_q as the primary signal and n_e and T_e as the secondary ones are shown below. Shown are the averaged fluctuating parts of E_q (solid), n_e (dashed) and T_e (dash-dot) normalized to corresponding RMS fluctuation levels.

REFERENCES

[1] P.C. Stangeby and G.M. McCracken 1990 *Nucl. Fusion* **30** 1225

[2] P.C. Liewer, J.M. McChesney, S.J. Zweben, and R.W. Gould 1986 *Phys. Fluids* **29** 309

[3] R.A. Moyer, J.G. Watkins, R.W. Conn, R. Doerner, D.N. Hill, R. Lehmer, R.T. McGrath, L. Schmitz, R.D. Stambaugh, G. Tynan 1992 *J. Nucl. Mater.* **196-198** 854

[4] R.A. Moyer, J.W. Cuthbertson, T.E. Evans, G.D. Porter, J.G. Watkins 1997 *J. Nucl. Mater.* **241-243** 663

[5] J.A. Boedo, P.W. Terry, D. Gray, R.S. Ivanov, R.W. Conn, S. Jachmich, G. Van Oost, and the TEXTOR Team 2000 *Phys. Rev. Lett.* **84** 263

[6] J. Watkins, J. Salmonson, R. Doerner, R. Lehmer, R. Moyer, L. Schmitz, D. Hill 1992 *Rev. Sci. Instrum.* **63** 4728

[7] J.C. Luxon, L.G. Davis 1985 *Fusion Technology* **8** Part 2A 441

[8] T. Rognlien et al 1992 *J. Nucl. Mater.* **196-198** 347

[9] H. Zohm 1996 *Plasma Phys. Control. Fusion* **38** 105

[10] J.G. Watkins, R.A. Moyer, D.N. Hill, D. Buchenauer, T.N. Carlstrom, R. Conn *et al* 1992 *J. Nucl. Mater.* **196-198** 829

[11] M. Wade *et al* 1999 *J. Nucl. Mater.* **266-269** 44

[12] J.A. Boedo, D. Rudakov, R. Moyer, S. Krasheninnikov, D. Whyte *et al* 2001 accepted for publication in *Phys. Plasmas*

[13] G. Antar, S. Krasheninnikov *et al* 2001 accepted for publication in *Phys. Rev. Lett.*

[14] L.L. Lao, H.St. John, R.D. Stambaugh, A.G. Kellman and W. Pfeiffer 1985 *Nucl. Fusion* **25** 1611

[15] J.A. Boedo, D. Gray, R.W. Conn, P. Luong, M. Schaffer, R.S. Ivanov, A.V. Chernilevsky, G. Van Oost and the TEXTOR Team 1999 *Rev. Sci. Instrum.* **70** 2997

[16] D. L. Rudakov, J. A. Boedo, R. A. Moyer, R. D. Lehmer, G. Gunner, J. G. Watkins 2000 *Rev. Sci. Instrum.* **72** 453

[17] D.W. Ross 1992 *Plasma Phys. Control. Fusion* **34** 137

[18] A. H. Nielsen, H. L. Pecsell, J. Juul Rasmussen 1996 *Phys. Plasmas* Vol.**3** No. **5** 1530

[19] R. D. Lehmer 1996 PhD thesis, University of California San Diego, UCSD-ENG-032

[20] A. V. Filippas, R. D. Bengtson, G. X. Li, M. Meier, CH. P. Ritz *et al* 1995 *Phys. Plasmas* 2 839

[21] M.V. Heller, Z.A. Brasilio, I.L. Caldas, J. Soteckel, J. Petrzilka 1999 *Phys. Plasmas* **6** 846

[22] G. Antar, P. Devynck, X. Garbet, S. Luckhardt 2001 *Phys. Plasmas* **8** 1612

[23] S. Krasheninnikov 2001 *Phys. Lett. A* **283** 368

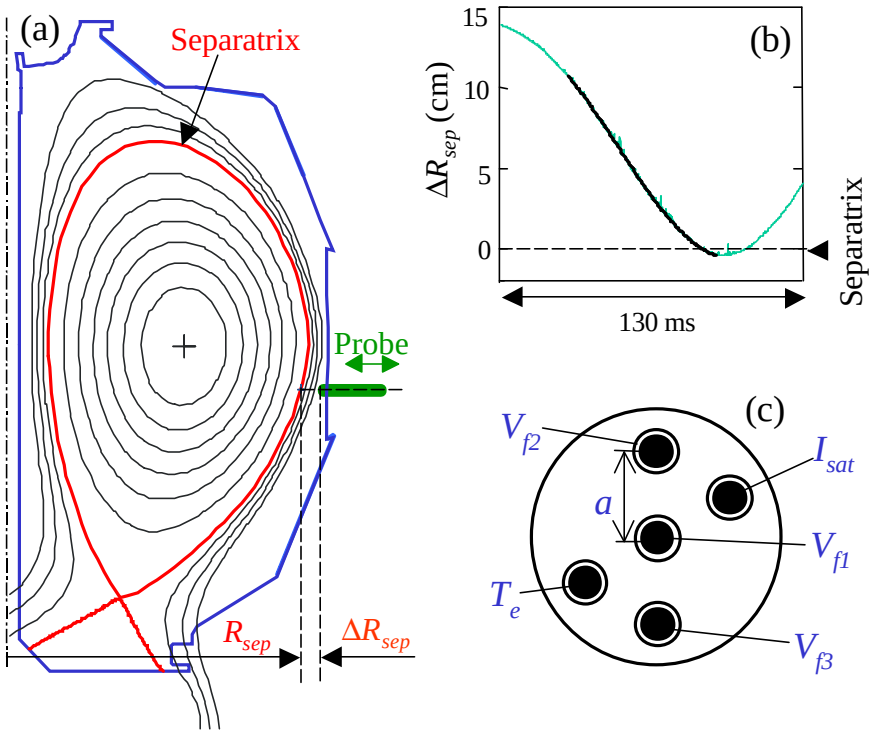
(a)
Separatrix
Probe
R_{sep}
ΔR_{sep}
(b)
15
10
5
0
ΔR_{sep} (cm)
130 ms
Separatrix
(c)
V_{f2}
I_{sat}
a
V_{f1}
T_e
V_{f3}

Figure 1

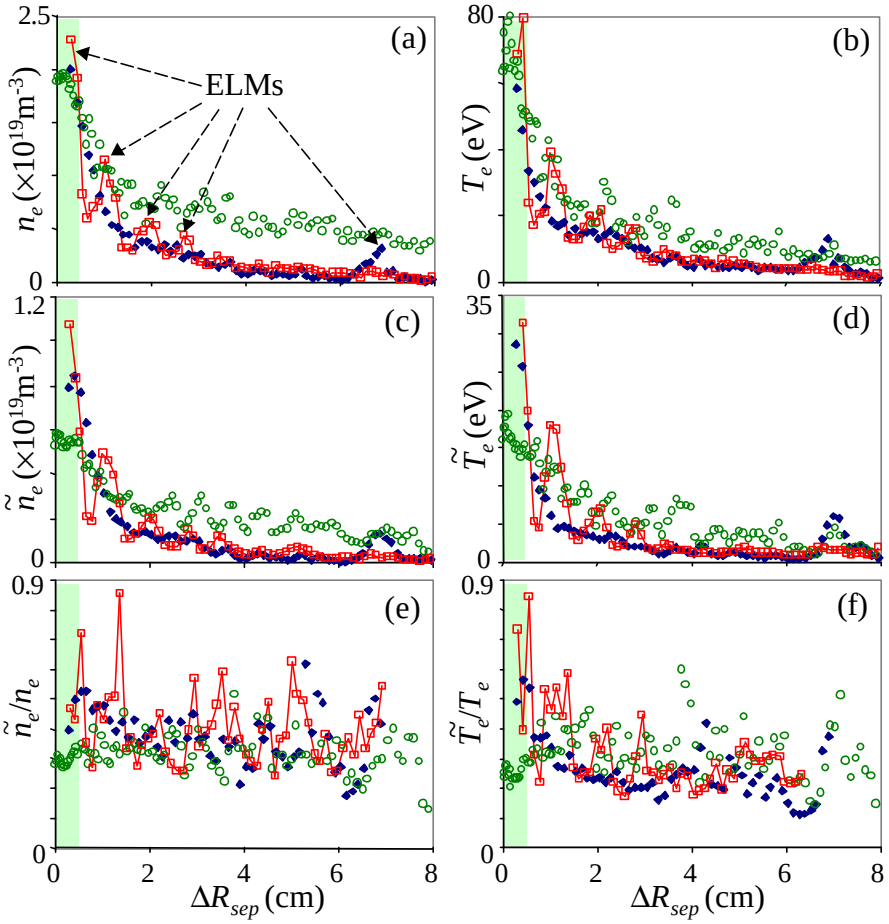
(a)
(b)
(c)
(d)
(e)
(f)
ELMs
2.5
0
80
1.2
35
0.9
n_e (×10^{19}m^{-3})
T_e (eV)
$\tilde{n}_e$ (×10^{19}m^{-3})
$\tilde{T}_e$ (eV)
$\tilde{n}_e/n_e$
$\tilde{T}_e/T_e$
0
2
4
6
8
ΔR_{sep} (cm)

Figure 2

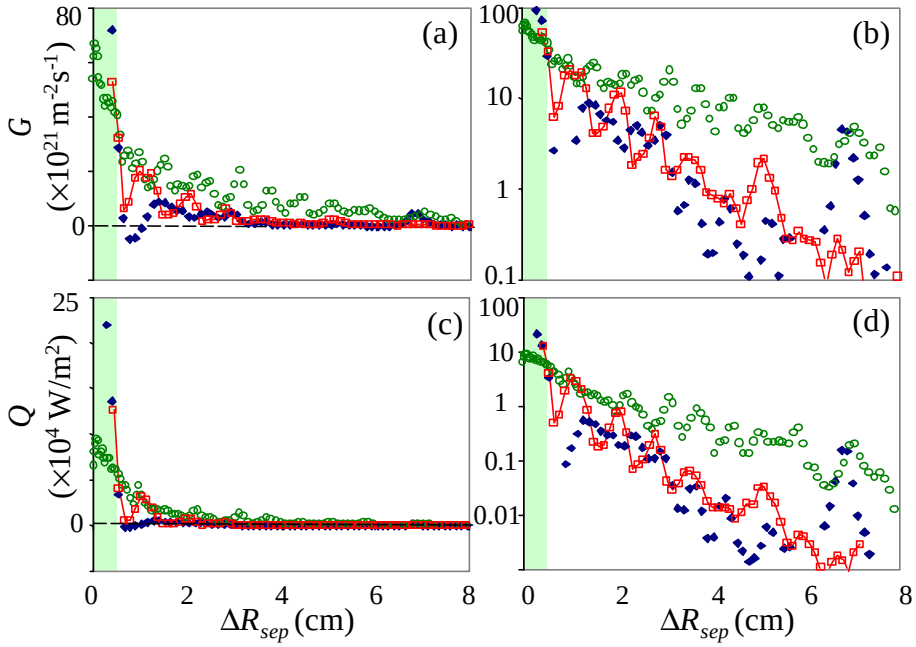

Figure 3

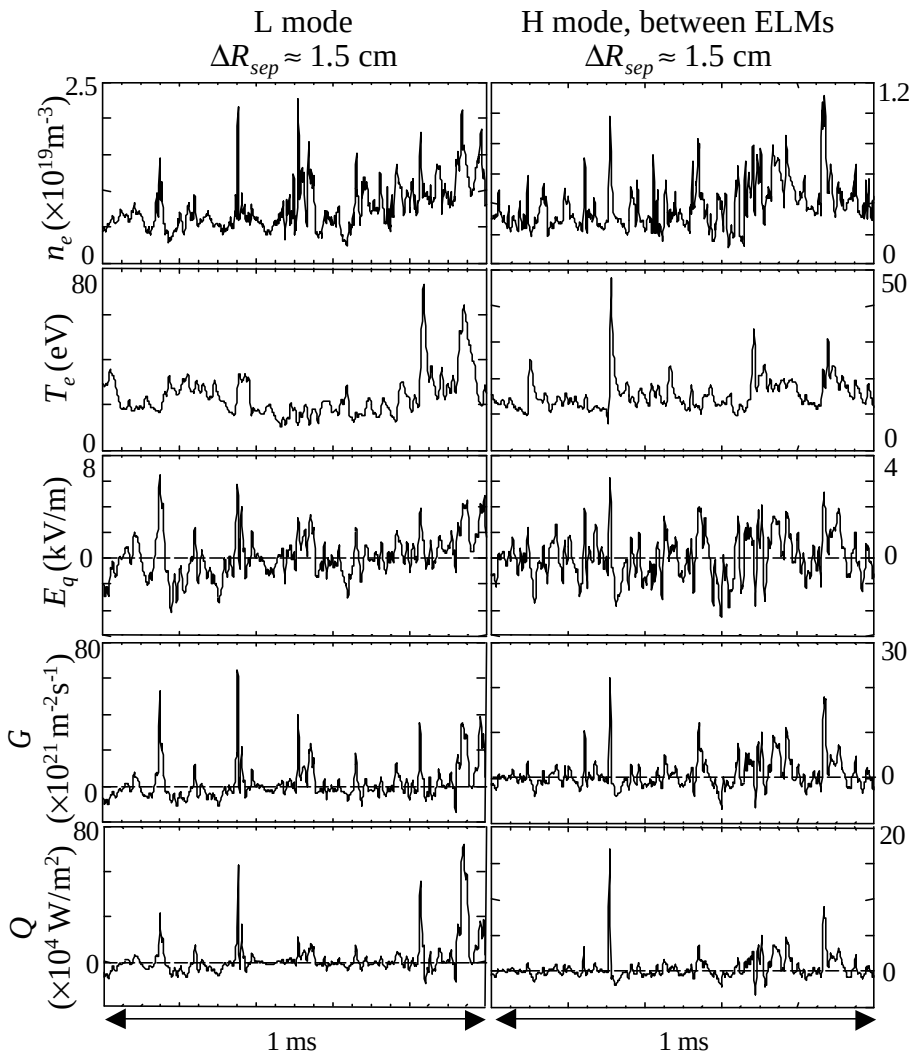
L mode
$\Delta R_{sep} \approx 1.5$ cm
H mode, between ELMs
$\Delta R_{sep} \approx 1.5$ cm
n_e ($\times 10^{19}$m^{-3})
2.5
0
1.2
0
T_e (eV)
80
0
50
0
E_q (kV/m)
8
0
4
0
G ($\times 10^{21}$m^{-2}s^{-1})
80
0
30
0
Q ($\times 10^4$ W/m^2)
80
0
20
0
1 ms
1 ms

Figure 4

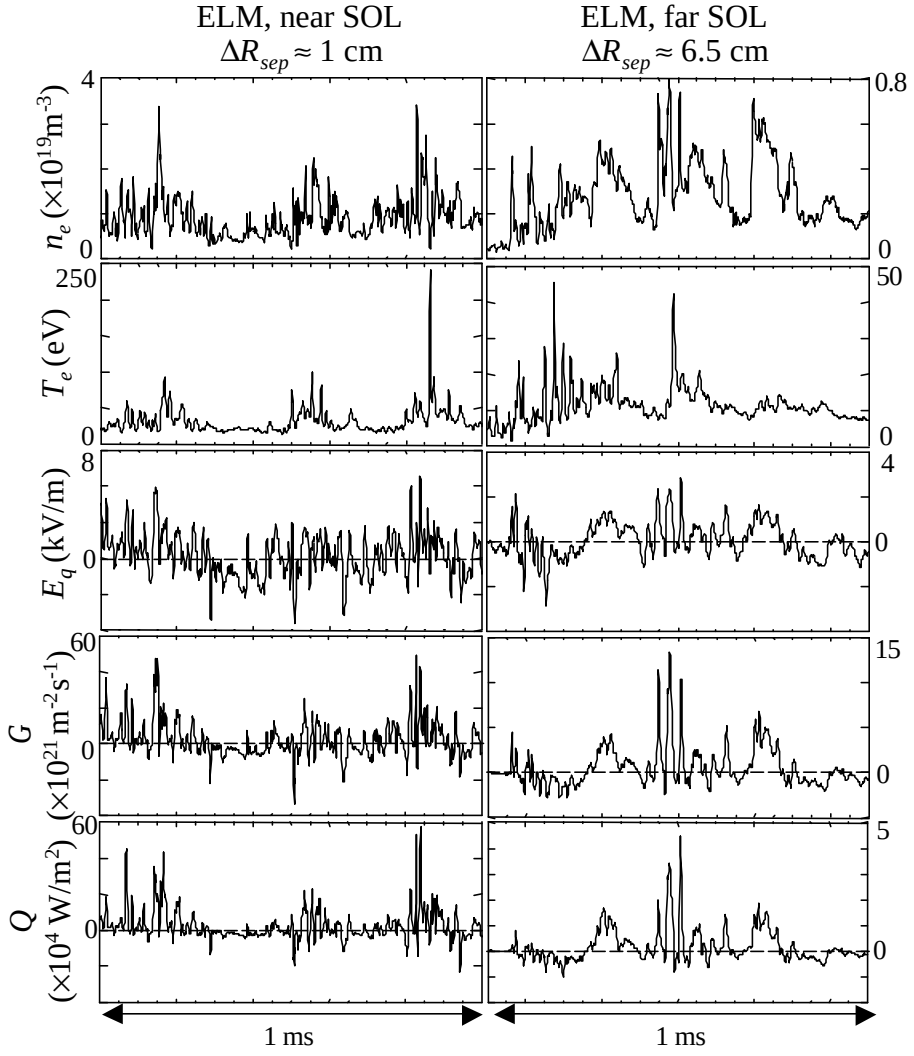
ELM, near SOL
$\Delta R_{sep} \approx 1$ cm
ELM, far SOL
$\Delta R_{sep} \approx 6.5$ cm
n_e ($\times 10^{19}$m^{-3})
4
0
0.8
0
T_e (eV)
250
0
50
0
E_q (kV/m)
8
0
4
0
G ($\times 10^{21}$ m^{-2}s^{-1})
60
0
15
0
Q ($\times 10^4$ W/m^2)
60
0
5
0
1 ms
1 ms

Figure 5

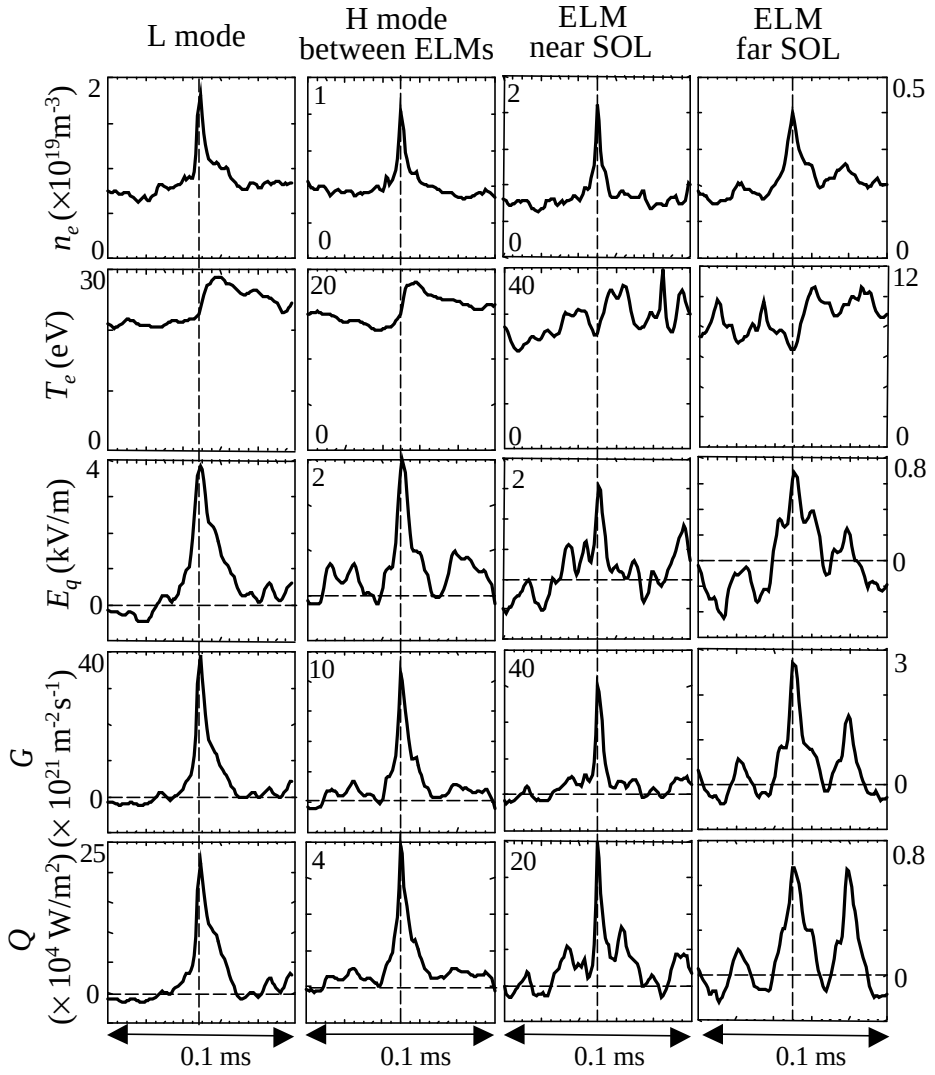
L mode
H mode between ELMs
ELM near SOL
ELM far SOL
n_e ($\times 10^{19}$m^{-3})
T_e (eV)
E_q (kV/m)
G ($\times 10^{21}$ m^{-2}s^{-1})
Q ($\times 10^4$ W/m^2)
0.1 ms
0.1 ms
0.1 ms
0.1 ms

Figure 6

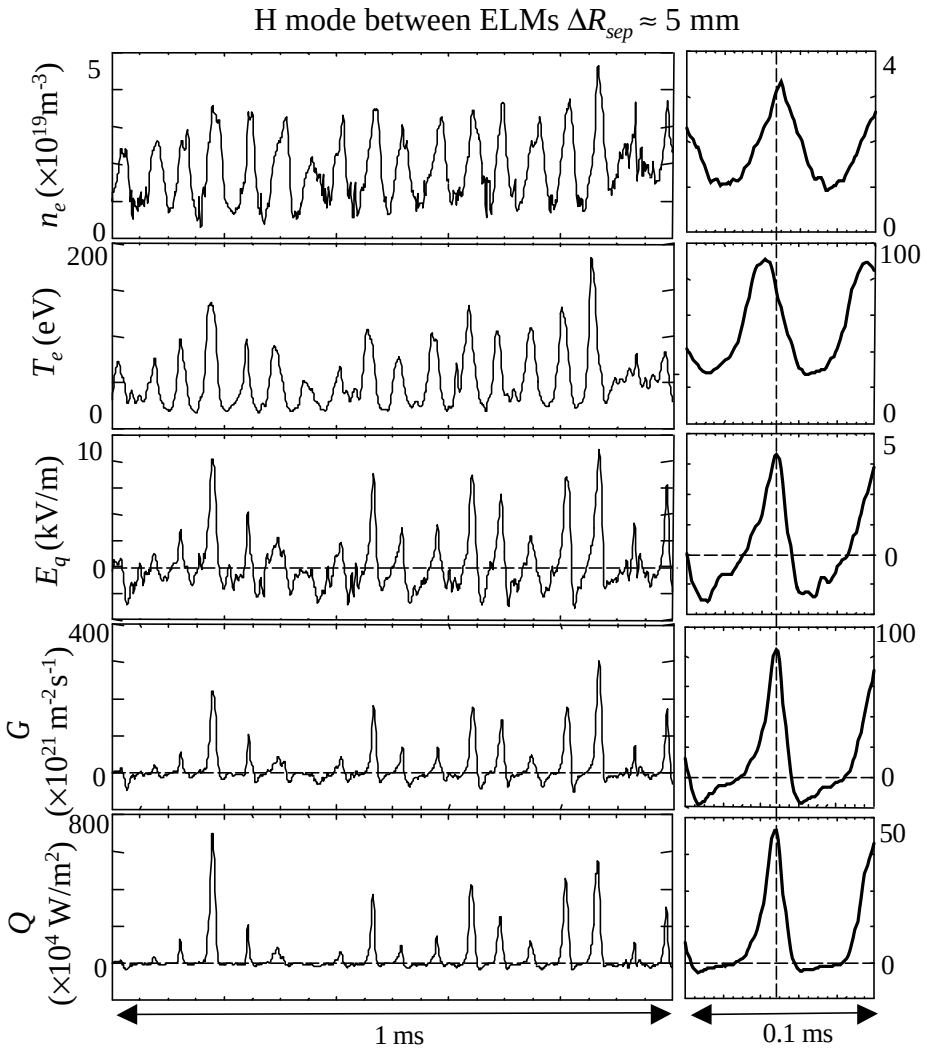
H mode between ELMs $\Delta R_{sep} \approx 5$ mm
n_e ($\times 10^{19}$m^{-3})
5
0
4
0
T_e (eV)
200
0
100
0
E_q (kV/m)
10
0
5
0
G ($\times 10^{21}$ m^{-2}s^{-1})
400
0
100
0
Q ($\times 10^4$ W/m^2)
800
0
50
0
1 ms
0.1 ms

Figure 7

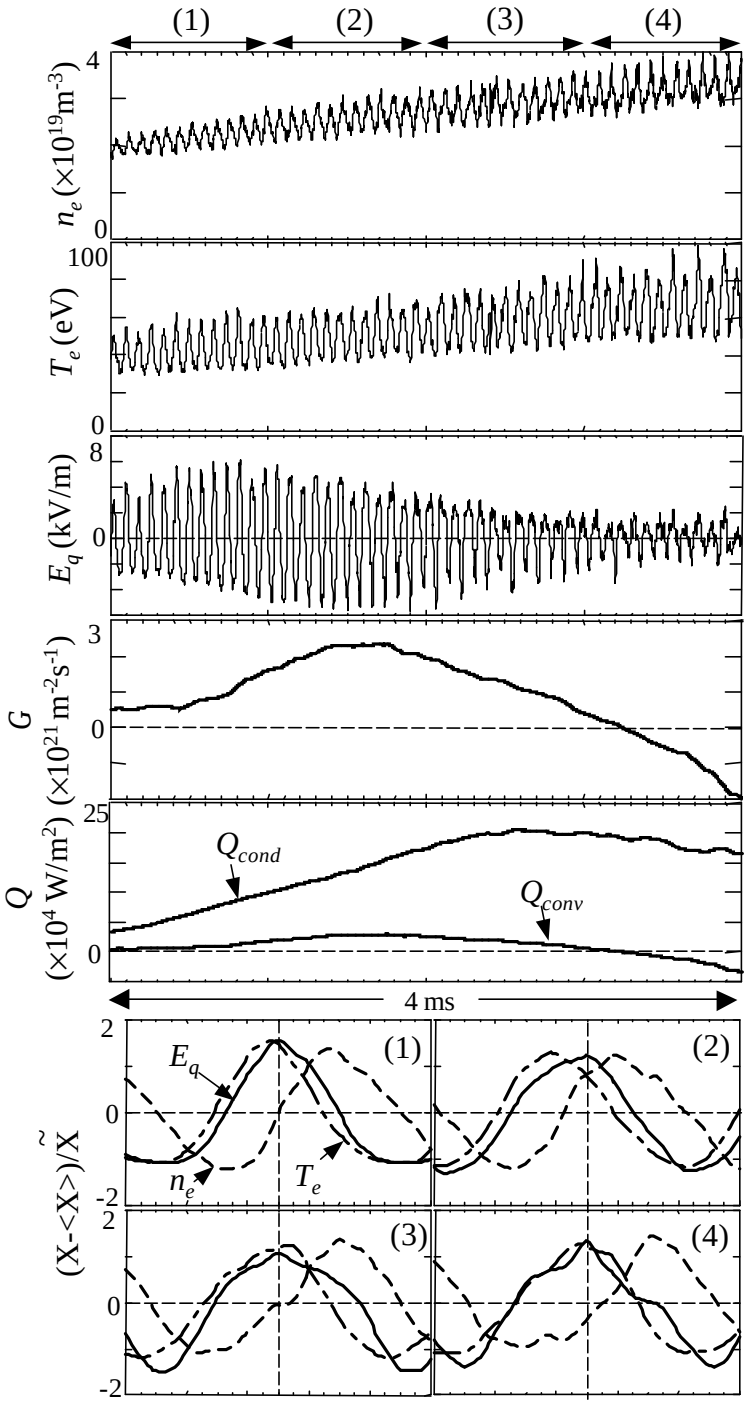
(1)
(2)
(3)
(4)
n_e (×10^{19}m^{-3})
4
0
T_e (eV)
100
0
E_q (kV/m)
8
0
G (×10^{21} m^{-2}s^{-1})
3
0
Q (×10^4 W/m^2)
25
0
Q_{cond}
Q_{conv}
4 ms
$\tilde{X}$/(X-<X>)
2
0
-2
E_q
n_e
T_e
(1)
(2)
(3)
(4)

Figure 8